CONCRETE LIBRARY OF JSCE NO. 34, DECEMBER 1999

SPATIALLY AVERAGED TENSILE MECHANICS FOR CRACKED CONCRETE AND REINFORCEMENT IN HIGHLY INELASTIC RANGE

(Reprinted from proceedings of JSCE, No.613/V-42, February 1999)

Hamed SALEM

Koichi MAEKAWA

The aim of this study is to obtain the spatial average stress-average strain relationships of both reinforcing bars and cracked concrete in RC members based on the local bond characteristics between concrete and reinforcing bars. The computation is capable of predicting the crack spacing and the ultimate average strain of reinforcing bars when total rupture takes place. A systematic verification through experimental work is conducted to clarify the versatility of the proposed model

Keywords: *Bond-slip-strain, tension stiffening, crack spacing*

Hamed M. M. Salem is an assistant professor at the Structural Engineering Department, Cairo University, Giza, Egypt. He obtained his Ph.D. from the University of Tokyo in 1998. After obtaining his Ph.D., he worked as a JSPS post-doctoral fellow in The Concrete Laboratory, The University of Tokyo. His research interests relate to nonlinear mechanics and the constitutive laws of reinforced concrete and seismic analysis of reinforced concrete. He is a member of the JSCE.

Koichi Maekawa is a professor at The University of Tokyo. He obtained his D. Eng. from the University of Tokyo in 1985. His research interests relate to nonlinear mechanics and the constitutive laws of reinforced concrete and seismic analysis of structures and concrete thermodynamics. He is a member of the JSCE.

---

1. INTRODUCTION

The tension stiffening effect represents the capacity of concrete to carry the internal tensile force that develops between adjacent cracks. In distinct cracked sections, the local tensile force is carried by both the steel reinforcing bars and the concrete residual softened tension. The force that develops in the reinforcement is partly transferred to the concrete between adjacent cracks through bond stress transfer between reinforcing bars and concrete, while the residual tensile stresses in crack sections act directly on the fracturing planes. The tension stiffening effect is usually treated by assuming a relationship between the average concrete tensile stress and the average concrete tensile strain over a long gauge length in the direction normal to the cracks (Shima et al.[4]).

At the same time, the stress-strain relationship of the reinforcement has to be treated on an averaged basis. Since the stress in a reinforcing bar embedded in concrete varies along its axis, the average stress-average strain relationship of the reinforcement is significantly different from the pointwise behavior of a bare bar after yielding (Shima et al. [4]). In fact, a bar starts to yield at the location of a concrete crack before any other point. Therefore, the spatial average yield stress is generally lower than the yield stress of a bare bar, as clearly pointed out by Okamura and Maekawa [5]. After yielding, some parts of the reinforcement close to cracks enter the strain-hardening zone, whereas other parts remain in the elastic zone. Therefore, the average response is a mix of elastic and hardening stiffness. Usually, a bilinear model is assumed for the average response of the steel bars.

Shima et al. [4] assumed that the reinforcing bar stress has a full cosine profile, and based on this distribution they obtained the average stress-average strain relationship for reinforcing bars. Their choice of a cosine stress distribution was based on the fact that the cosine function is symmetric and its derivative is zero at both the cracked section and the center of the segment. This agrees well with the fact that the bond stresses at the cracks and at the midway points between two successive cracks are zero.

Belarbi and Hsu [6] assumed a different stress profile consisting of the summation of Shima's cosine function and two other sinusoidal functions. The purpose of this modification was to simulate the fact that, after reinforcing bars yielding, the bond stress between reinforcing bars and concrete deteriorates and the reinforcing bar stress in the vicinity of the cracks becomes uniform.

The assumptions made by both Shima and Belarbi are acceptable for medium and highly reinforced concrete, where the spacing of cracks is relatively small. However, for lightly reinforced concrete, the crack spacing is larger and tends to be localized much as in plain concrete. In this case, both Shima and Belarbi's stress distributions are no longer valid and the local steel stress has to be computed from micro-bond characteristics.

The importance of considering tension softening in cracked sections also arises in lightly reinforced concrete, as its contribution becomes higher compared to the contribution of bond stress transfer. In this study, the microscopic bond stress transfer and tension fracturing of plain concrete are coupled. The local stresses and strains of steel and concrete are computed, and hence the macroscopic behavior is evaluated.

In Shima and Belarbi's modes, the stress profile between cracks is assumed to be similar, so bond deterioration is taken into account only indirectly and the absolute value of crack spacing is not necessarily incorporated. However, over the past decade, there has been some progress in the understanding of bond deterioration close to crack planes (Qureshi and Maekawa [8]) and the fracturing process at a crack section. The authors therefore judged that it is the right time to re-formulate the average-based tension model of cracked concrete and embedded reinforcement, using a direct theoretical derivation from microscopic mechanics. In computing the critical ductility, when the steel ruptures inside the concrete, a microscopic approach is indispensable since the rupture criterion is set for the local behavior of the steel. Furthermore, RC ductility in the case of low reinforcement ratios is of great importance in estimating the seismic performance of existing large-scale structures. Low reinforcement cases in which the simplified stress profile cannot be applied have long been of interest to engineers involved in seismic analysis.

The present tension-stiffening model proposed by Shima et al [4] is an empirical one and does not take into consideration the amount of reinforcement. As a matter of fact, the experimentally obtained tension stiffening of cracked concrete is hardly affected by the reinforcement ratio (Okamura and Maekawa [5]). However, the amount of reinforcement has a considerable effect on the tension stiffening of lightly reinforced members. In the present study, the tension stiffening is also analytically computed and the effect of the amount of reinforcement is quantitatively taken into account. The aim of this study is to obtain a versatile smeared tension model for reinforcing bars and concrete in both heavily and lightly reinforced concrete. At the same time, the average crack spacing and the average ultimate stress are computed.

2. SPATIAL-AVERAGED CONSTITUTIVE LAWS IN TENSION

(1) Bond-slip-strain model

Shima et al. [4] proposed a universal bond stress-axial slip-steel strain model for RC. The model offers a unique relationship that expresses the bond characteristics as derived from both pullout and axial tension tests. The authors adopt this model for the local stress interaction between concrete and reinforcement as,

$$\tau(\varepsilon, s) = \tau_0(s)\, g(\varepsilon) \tag{1}$$

where, $\tau(\varepsilon, s)$ is the local bond stress and $\tau_0(s)$ is the intrinsic bond stress when the strain is zero and denoted by,

$$\tau_0(s) = f_c'\ k\,[\ln(1+5s)]^{c} \tag{2}$$

$$g(\varepsilon) = \frac{1}{1+10^5\varepsilon} \tag{3}$$

where, f_c' is the compressive strength of the concrete, k is constant=0.73, c is constant=3, s is the non dimensional slip =1000S/d, S is slip, and d and ε are the diameter and strain of the bar.

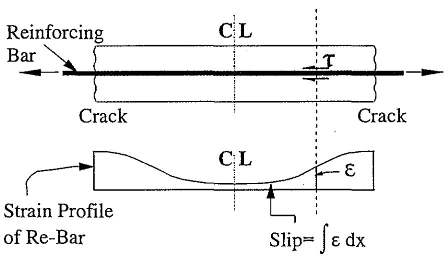

Fig. 1 Definition of slip in bond-slip-strain model (Shima et al.[4])

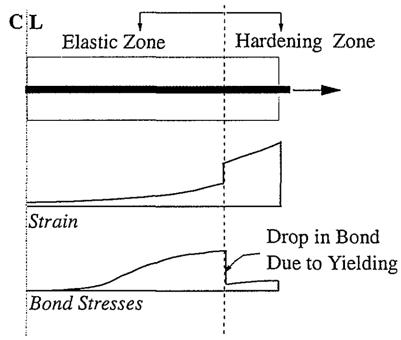

Fig. 2 Bond stresses in the post-yielding range

Figure 1 shows the parameters used in the model. The model is applicable to both the elastic range and the post-yield range (Shima et al. [4]). Using this model, the phenomenon of bond reduction in the post-yield range can be coherently explained. When the reinforcing bar starts to yield, in the vicinity of a crack, the strain suddenly increases to the strain hardening zone leading to a drastic drop in the strain function denoted by $g(\varepsilon)$ in **Eq. 3**. However, the slip function may be unchanged since the slip rises little since the integrated strain, which is equivalent to the slip, remains almost the same because the plastic region just after yield is so limited. This drop in the strain function causes a fall in the bond stress as shown in **Fig. 2**. It should also be noted that local bond in the post-yield range of the steel is apparently influenced by the stress-strain characteristics and elasticity of the bare bar. The drop in bond stress of reinforcement with a short yield plateau is expected to be less than that of reinforcement with a long yield plateau. This qualitative feature of the bond mechanism can be systematically treated in the use of the local bond-slip-strain model. The authors chose to accept this scheme in their investigation.

(2) Bond Deterioration Model

When a reinforcing bar is tensioned against concrete, the lugs of the reinforcing bar act against the concrete and cause conical diagonal compressive struts (Goto [1]). Tensile stresses are generated in a direction perpendicular to these struts, causing splitting conical cracks. In the vicinity of the crack planes, these struts have no concrete to support because the cracks penetrate to the crack planes. Therefore, concrete spalling easily occurs, resulting in bond deterioration as shown in **Fig. 3** (Qureshi and Maekawa [8]). Shima's model cannot be applied to the bond deterioration zone where the "near crack surface effect" is predominant (Okamura and Maekawa [5]).

In fact, the localization of plastic yielding is initiated at the bond deterioration zone. Thus, the modeling of the bond close to cracks plays an important role in the analysis of the post-yield behavior of RC in tension. Qureshi and Maekawa [8] assumed in their RC joint model that the bond stress linearly decreases to zero at a distance 5 d (d is defined as the bar diameter) from the crack surface, and that the bond stress drops suddenly to zero at a distance 2.5 d from the crack surface due to concrete splitting and crushing around the bar beside the crack surface. **Figure 3** shows a schematic drawing of the bond deterioration model, which describes,

$$\tau(x) = \tau_{max} - \frac{\tau_{max}}{L_b}\left[x - \left(\frac{L_c}{2} - L_b\right)\right], \quad \frac{L_c}{2} - L_b \le x \le \frac{L_c}{2} - \frac{L_b}{2} \tag{4}$$

$$\tau(x) = 0 \quad , \quad \frac{L_c}{2} - \frac{L_b}{2} \le x \le \frac{L_c}{2} \tag{5}$$

However, an important consideration is that when the crack spacing falls below 10d, the bond deterioration length cannot logically equal 5d as the splitting conical cracks cannot physically intersect. Also, when the crack spacing falls below 5d, concrete spalling cannot happen. Consequently, it was assumed that the bond deterioration length is equal to zero when the crack spacing is less than 5d, and it changes linearly from zero to 5d when the crack spacing changes from 5d to 10d as shown in **Fig. 4**. Nevertheless, this situation rarely occurs and only in cases where the reinforcement ratio is very high and the tensile strength is so small.

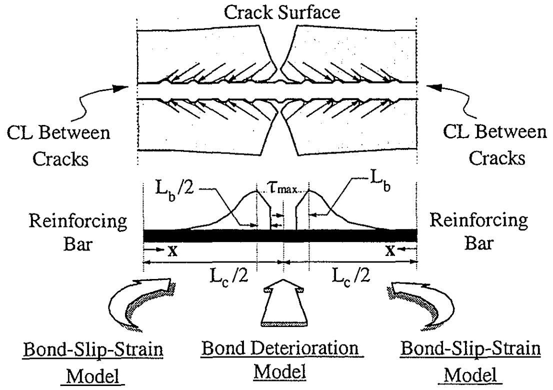

Fig. 3 Bond deterioration close to cracks (Qureshi and Maekawa [8]).

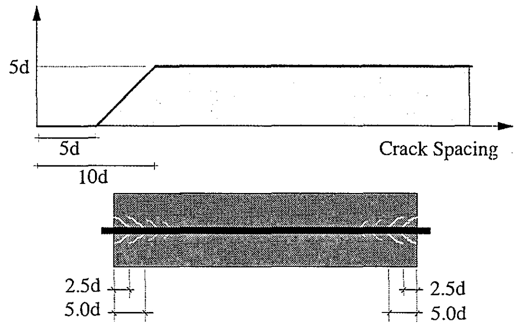

Fig. 4 Modification of bond deterioration model for small crack spacing

(3) Tension Softening at Crack Surface

When concrete cracks, the stress carried by the concrete at the crack surface does not drop to zero suddenly. The interlocking of the two faces of the crack causes a transfer of some residual stresses. This phenomenon is known as tension softening of plain concrete. Regarding reinforced concrete members with ordinary reinforcement ratios, this softening can be neglected compared to the force carried by bond stress transfer.

However, in the case of small reinforcement ratios, this softening may not be neglected. To study the effect of tension softening coupled with RC behavior, a combination of fracturing softening and bond tension stiffening is a fruitful approach. Usually, tension softening is expressed as a relationship between the residual tensile stress and the crack width, which is the main parameter of the tension softening phenomenon. The surface crack width can be considered being compatible with the reinforcement slip at the crack. Thus, the surface crack width is equal to the sum of bar slip on both sides of the crack. In other words, the surface crack width is equal to twice the reinforcement slip, on one side at the crack location. The average crack width used by Qureshi and Maekawa [8] is adopted here:

$$w = C(2S_{max}), \quad S_{max} = S|_{x=L_c/2} \tag{6}$$

where C is equal to (1/1.3). The tension softening model adopted in the analysis (Uchida et al. [7]) is defined as,

$$\sigma_{br} = f_t\left[1+0.5\left(\frac{f_t}{G_f}\right)w\right]^{-3} \tag{7}$$

where, σ_{br} is the bridging stress across the crack, f_t is the tensile strength, w is the crack width, and G_f is the fracture energy and ranges from 0.1 to 0.15 N/mm for plain concrete [7].

3. LOCAL ANALYSIS AND AVERAGING

In order to obtain the steel stress profile, other governing equations have to be simultaneously solved. By dividing the portion of the reinforcing bar between two adjacent cracks into infinitely small segments and satisfying the static equilibrium of all elements, we obtain the first of these, the following continuum equilibrium equation:

$$\frac{d\sigma}{dx} = \frac{\pi d}{A_s}\tau \Rightarrow \frac{\Delta\sigma}{\Delta x} = \frac{\pi d}{A_s}\bar{\tau} \text{ (in computation)} \tag{8}$$

where, $d\sigma/dx$ is the axial stress gradient along the axis of the reinforcing bar, As and d are the cross-sectional area and diameter of the reinforcing bar, and $\bar{\tau}$ is the average bond stress.

The second equation to be solved is the bond-slip-strain model **(Eq. 1, 2, and 3)**, together with the bond model in the bond-deterioration zone **(Eq. 4 and 5)**. The third equation derives from the slip compatibility. The slip is computed by integrating the strain over the length of the reinforcing bar starting midway between adjacent cracks, as shown in **Fig. 1**, i.e. the slip at the midway point between cracks is zero. Thus, we have,

$$S(x) = \int_0^x \varepsilon dx \tag{9}$$

The fourth equation is the constitutive equation for the bare bar, which represents the point-wise relationship between the reinforcing bar stress and strain at each bar section obtained from the uniaxial stress-strain relation of the bar used as,

$$
\begin{aligned}
\sigma &= E_s \varepsilon \quad , 0 < \varepsilon < \varepsilon_y \\
\sigma &= f_y \quad , \varepsilon_y \leq \varepsilon < \varepsilon_{sh} \\
\sigma &= f_y + \{1 - e^{(\varepsilon_{sh}-\varepsilon)/k}\}(1.01 f_u - f_y) \ , \varepsilon > \varepsilon_{sh} \\
k &= 0.032(4000/f_y)^{2/3}
\end{aligned}
\tag{10}
$$

The overall scheme of the computation is summarized in **Fig. 5** and **Fig. 6** [10), 11)]. Firstly, the crack spacing is equal to the total length of the target control volume. The load is increased gradually and local stresses in both concrete and steel are computed. When the maximum local concrete stress exceeds the tensile strength of the concrete, a new crack is introduced in the middle of specimen. Computations are carried out again with a crack spacing equal to half the initial bar length. The new crack spacing is in fact the average crack spacing, since the real location of the crack is not necessarily in the middle of the specimen. The location of the crack depends on the distribution of local tensile strength along the length of the specimen. Due to the non-uniformity of concrete, tensile strength varies along the specimen length. For simplicity however, an average crack spacing is assumed.

Again, the load is increased gradually and the local concrete stresses are checked. When the concrete stress exceeds the tensile strength, another new crack is introduced in the middle of one of the two halves of the specimen and the average crack spacing is now one-third of the initial length, as shown in **Fig. 5**. The new crack occurs in only one half, since in reality it is not possible for two cracks to develop simultaneously. This is experimentally verified by the fact that the maximum crack spacing is twice the minimum crack spacing (Goto [1)], and Rizkalla [3)]). After the formation of the second crack, it is possible for the third crack to talk place in the other half of the specimen. Following the same concept, cracks are generated until the stable state is reached. At this moment, no new cracks are generated, and it arises after yielding of the reinforcement due to a drastic drop in the bond stresses.

To compute stress profiles, a finite discretization of the reinforcing bar between two successive cracks is performed, as shown in **Fig. 5** and **Fig. 6**. Starting from the midway point between two adjacent cracks, a finite segment of length Δx is studied. The boundary conditions for this segment are set by equating both the slip and the bond stress at the middle section to zero, and assuming an arbitrary value of strain at the middle. This arbitrary strain value represents the loading level. The four equations are simultaneously solved using an iterative procedure. Upon finishing the computation for this segment, the boundary conditions of the next division are defined and a similar computation procedure is followed. Hence, the strain and stress profiles of the steel reinforcement can be drawn. It results in the steel average stress and average strain as,

$$\bar{\varepsilon} = \frac{2}{L_c}\int_0^{\frac{L_c}{2}} \varepsilon(x)dx \cong \frac{2}{L_c}\sum_0^{\frac{L_c}{2}} \varepsilon(x)\Delta x \tag{11}$$

$$\bar{\sigma}_s = \frac{2}{L_c}\int_0^{\frac{L_c}{2}} \sigma_s(x)\,dx \cong \frac{2}{L_c}\sum_0^{\frac{L_c}{2}} \sigma_s(x)\Delta x \tag{12}$$

By computing the stress profile of the reinforcement, the stress profile of the concrete is obtained by subtracting the reinforcement force profile from the reinforcing bar force in crack. Adding the bridging stress defined by **Eq. 7**, the average stress of the concrete is mathematically defined as,

$$\bar{\sigma}_c = \sigma_{br} + \frac{2}{L_c}\int_0^{\frac{L_c}{2}} \sigma_c(x)\,dx \cong \sigma_{br} + \frac{2}{L_c}\sum_0^{\frac{L_c}{2}} \sigma_c(x)\,\Delta x \tag{13}$$

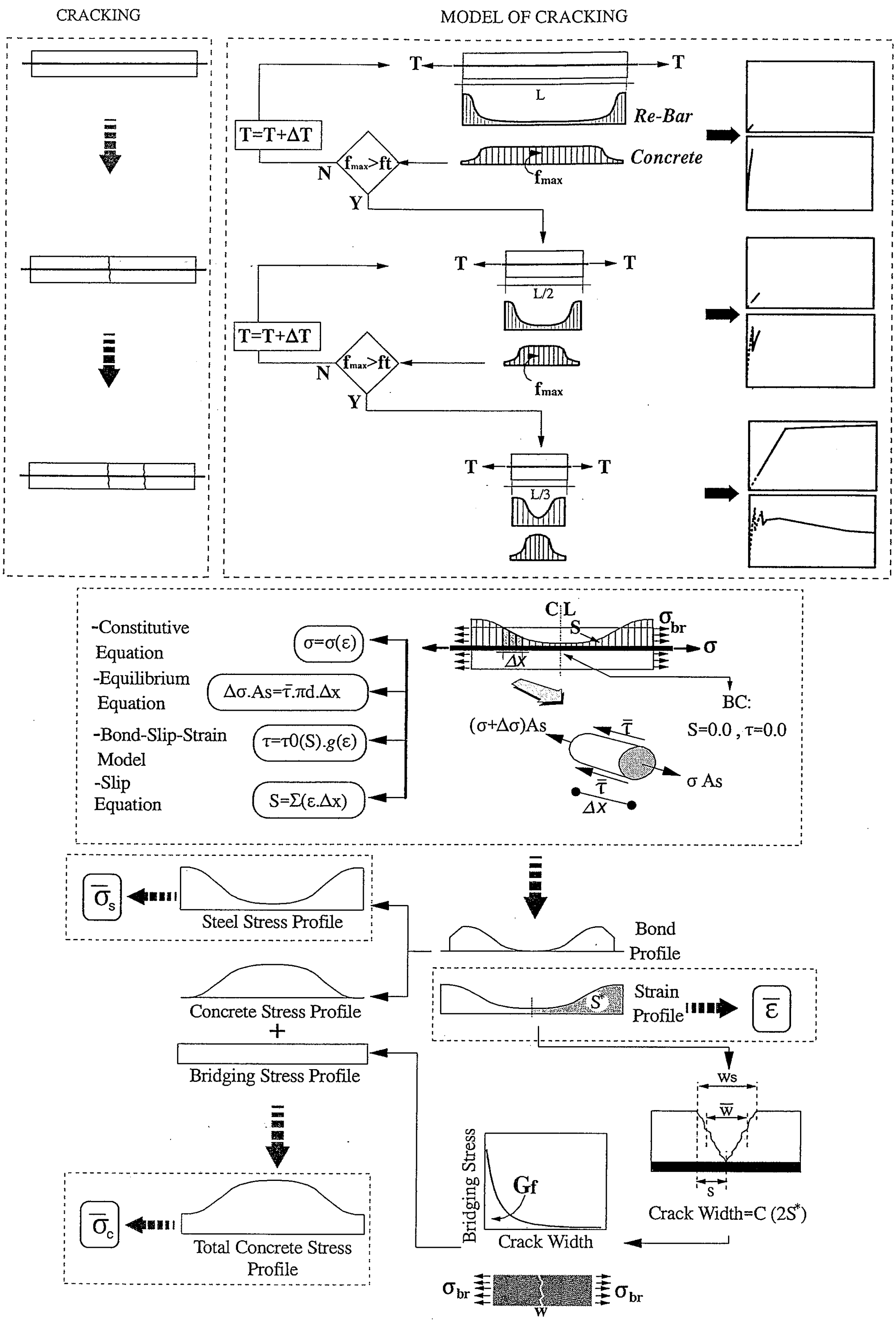

Fig. 5 Scheme for solving bond governing equations with finite discretization

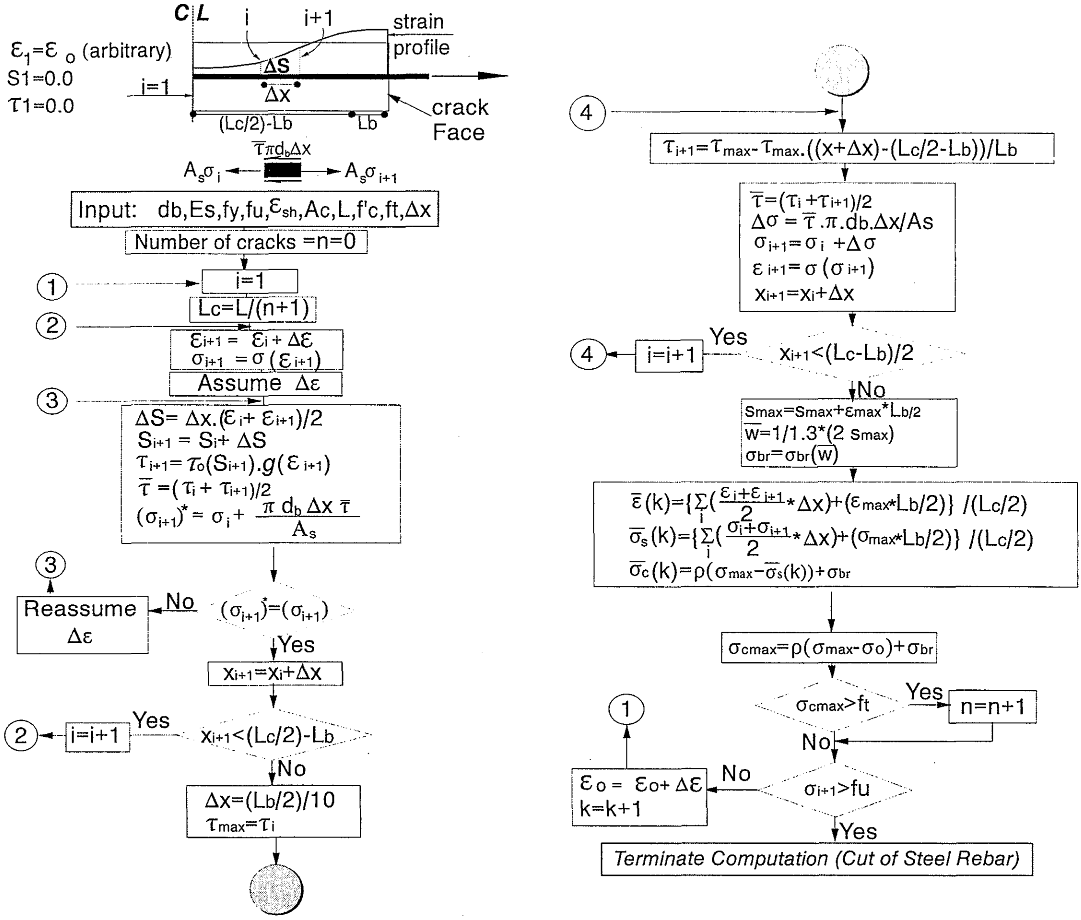

Fig. 6 Flow chart for solving bond governing equations with finite discretization

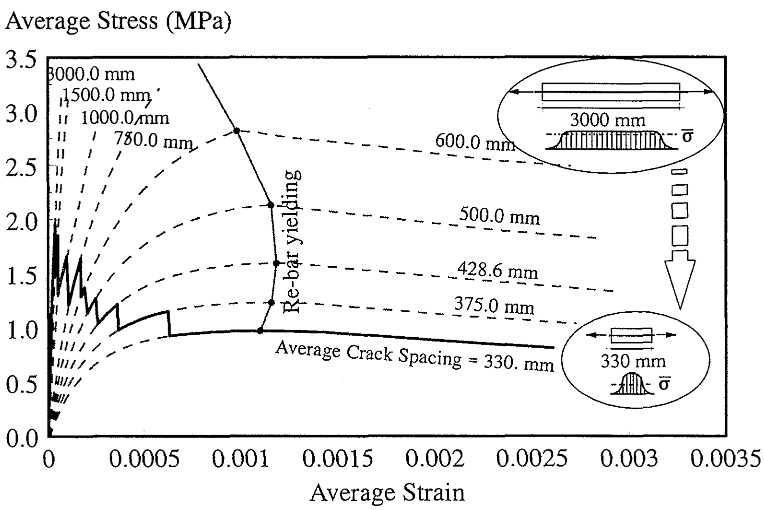

Fig. 7 Cracking of concrete

Figure 7 provides a deeper understanding of the cracking behavior and the tension stiffening of concrete. The dashed curves represent the average stress-average strain relationship of concrete for different crack spacings considering no cracking at all and the solid curve represents the behavior when cracking is considered in the scheme proposed here. The initial specimen length is 3,000 mm, and the final crack spacing is 330 mm. When a certain crack spacing is considered, the typical curve comprises two major parts, and these are connected by a point representing the initiation of reinforcement yielding. Before yielding of the reinforcement, the average stress of the concrete is an ascending line, whereas after yielding it falls. This is due to the fact that the bond stress suddenly decreases after yielding, resulting in a decrease in the load carried by the concrete. Once this point is reached, it is highly likely that no more cracks will be generated because of the reduced force transferred to the concrete. In the example shown in **Fig. 7**, yielding starts when average crack spacing reaches 330 mm, and no more cracks are computationally generated. Hence, the final crack spacing is designated as 330 mm.

In carrying out the analysis, however, it was found that when the cracking load of the concrete is close to the reinforcement yielding load, which is mainly the case with low reinforcement ratios, cracking may occur after yielding. This is due to the fact that when the cracking load is close to the yielding load, the crack spacing is relatively larger. As a result, the plasticity zone close to cracks is relatively small compared to the crack spacing. Hence, even though the average concrete stress falls after yielding, on the local level far from the crack surface, the local concrete stress may still increase and lead to new cracks.

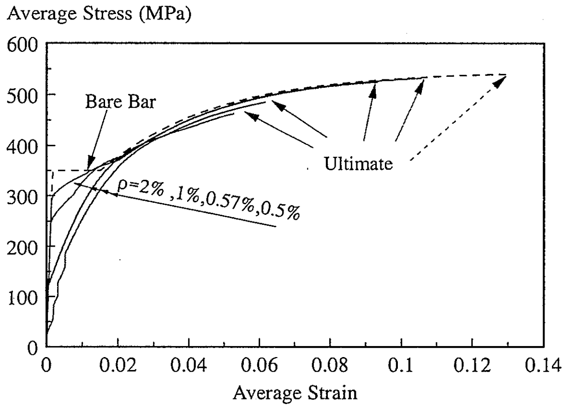

Fig. 8 Average response of reinforcement with different reinforcement ratios

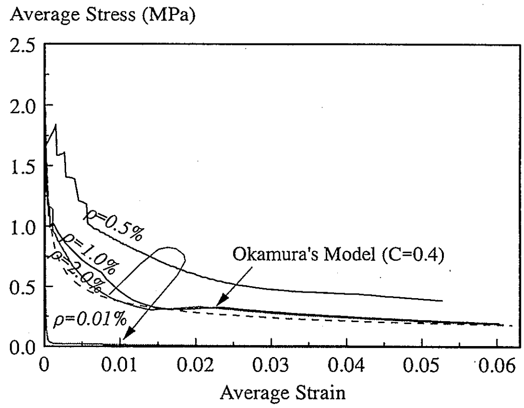

Fig. 9 Average response of concrete with different reinforcement ratios

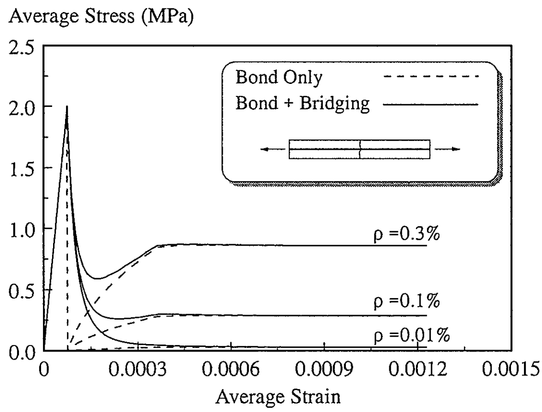

Fig. 10 Tension softening effect on tension stiffening of RC with low reinforcement ratios

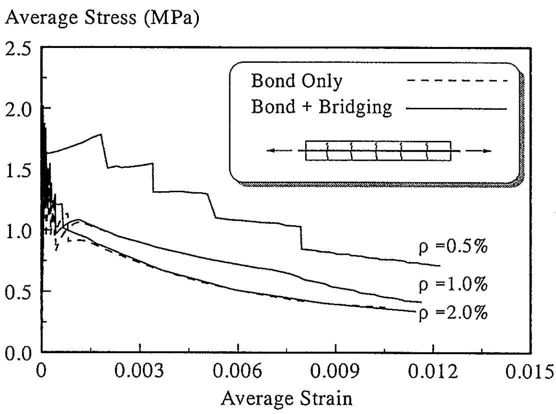

Fig. 11 Tension softening effect on tension stiffening of RC with ordinary reinforcement ratios

Figure 8 shows the average response of the reinforcement at different reinforcement ratios compared to the behavior of a bare bar. In this analysis, the ultimate average strain is defined as the average strain at which the local steel stress at the cracked section reaches the ultimate local stress. In this figure, it can be seen that the average yield stress falls with the decrease in reinforcement ratio. It is also obvious that the higher the reinforcement ratio, the higher the ultimate average strain, i.e. the higher ductility.

Figure 9 shows the average tensile response of concrete for different reinforcement ratios in comparison with the current model of Okamura and Maekawa [5]. It can be seen that this analysis agrees with the model in the case of normal reinforcement ratios of around 1 and 2%. However, for light reinforcement close to the minimum level specified in the codes, the macro model underestimates the tension stiffening of concrete. In case of a very small reinforcement ratio or plain concrete, the model on the contrary overestimates the tension stiffening. This means that the current tension stiffening model is reasonably valid in the case of ordinary reinforcement ratios, but it requires more versatility to cope with varying reinforcement ratios and material strengths.

Figures 10 and **11** illustrate the analysis of two groups, one with low reinforcement ratios where only one crack is computed and the other with ordinary reinforcement ratios where several cracks are predicted. For the low reinforcement ratio group, the contribution of the bridging stresses is significant. Increasing the reinforcement ratio leads to an increased contribution by bond compared to the bridging stress even in the one-crack case. The bridging stress can be neglected as compared with the bond contribution in the high reinforcement group, as shown in **Fig. 11**.

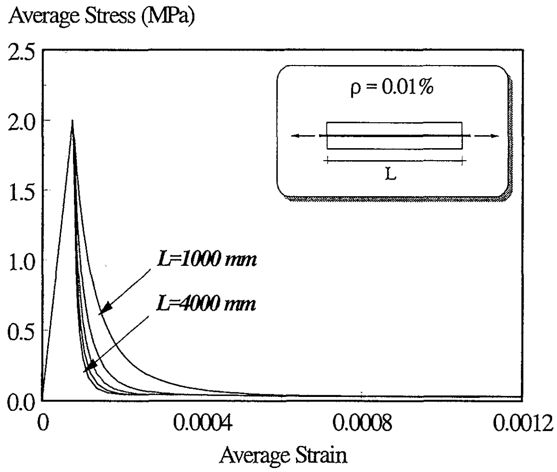

Fig. 12 Size effect on average response of concrete with very low reinforcement ratios

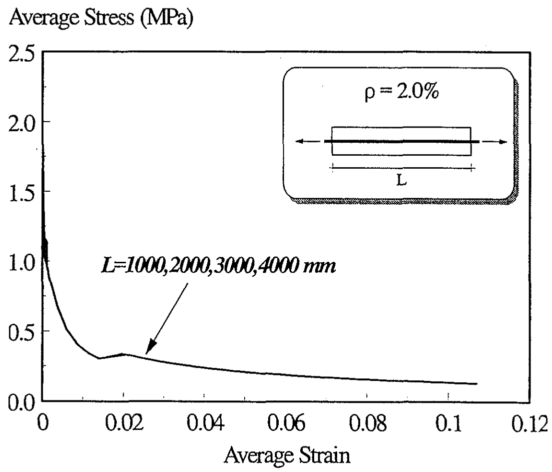

Fig. 13 Size effect on average response of concrete with ordinary reinforcement ratios

Figures 12 and **13** shows the gauge length effect on the average response of the concrete. Comparing two cases, one with heavy reinforcement and the other with light reinforcement, it can be seen that tension stiffening is more stable and independent on gauge length in the case of heavy reinforcement, while it depends very much on gauge length in the case of a low reinforcement ratio or plain concrete. In fact, this is due to the localization of cracks in lightly reinforced concrete, leading to behavior similar to that of plain concrete and the average response becomes dependent on the gauge length. On the other hand, for reinforced concrete with a high reinforcement ratio, cracking is controlled by the reinforcement through the bond mechanism, resulting in an almost equal crack spacing no matter how different the gauge lengths are.

4. EXPERIMENTAL VERIFICATION

(1) Comparison with the Experimental Work of Belarbi and Hsu [6]

As a verification of this analysis, a comparison with the experimental work conducted by Belarbi and Hsu [6] was carried out. The experiments were carried out on full-size reinforced concrete panels 1,400 × 1,400 × 180 mm. Specimens were first subjected to tension in the horizontal direction. After attaining a designated average tensile strain in the panel, compressive stresses were gradually applied in the vertical direction until failure while maintaining the average tensile strain developed in the initial testing phase. A comparison of the authors' analysis with those experiments is shown in **Fig. 14**. The analysis of Belarbi and Hsu [6] is plotted on the same graph. The author's analysis seems to be better than Belarbi's, especially in panel E4-0.5 with a reinforcement ratio of 0.5%. In fact, the reinforcement ratio in this panel is low, resulting in a relatively large crack spacing and a stress distribution far from that proposed by Belarbi.

(2) Comparison with the Experimental Work of Shima et al. [4]

Another verification of the analysis is carried out through a comparison with the experimental work conducted by Shima et al. [4] as shown in **Figs. 15, 16,** and **17**. The tested specimens were 2700 mm in length. This length was selected as long enough to correctly represent the average response since a longer specimen, which includes more cracks, will give higher accuracy. Cross sections of 150 × 200 mm and 200 × 250 mm were used. A deformed steel bar having a diameter of 19 mm was used and the reinforcement ratio was adjusted by changing the cross-sectional area of concrete. The authors' analysis agrees well with the reality.

(3) Authors' Test Specimens

a) Introduction

The specimens tested by Shima et al.[4] were loaded up to an average strain of 1~2%, and were not loaded to failure. Further, no specimens with very low reinforcement ratios, where the cracking behavior is localized, were tested.

As a completion and complement to Shima's experimental work, the authors tested 3 specimens, of which two were loaded up to failure. The reinforcement ratios of 2 specimens were selected to be slightly larger than the critical reinforcement ratio and the third was smaller than the critical reinforcement ratio, which is defined as,

$$\rho_{cr} = \frac{f_t}{f_y} \tag{14}$$

When the reinforcement ratio equals the critical reinforcement ratio, the yielding load equals the cracking load. If the reinforcement ratio is less than the critical reinforcement ratio, the behavior of reinforced concrete is expected to be similar to that of plain concrete and cracking will be localized. In other words, once the first crack occurs, the reinforcement starts to yield and no more cracks or certainly few cracks are generated.

b) Specimens

Figure 18 shows details of the specimens and the mounting of displacement transducers. The length of the specimens was 1,700 mm. This was the longest possible within the limitations of the laboratory facilities. The cross section of all specimens was 100 × 100 mm. A deformed reinforcing bar was used and no stirrups were incorporated. Specimens 1 and 2 were reinforced with a 10 mm deformed bar, whereas specimen 3 was reinforced with a 6 mm deformed bar. The reinforcement ratio of specimens 1 and 2 was 0.75%, a value slightly larger than the critical reinforcement ratio, whereas that of specimen 3 was 0.32%, which was less than the critical reinforcement ratio. A 30mm coupler was attached to the end of reinforcing bar at the

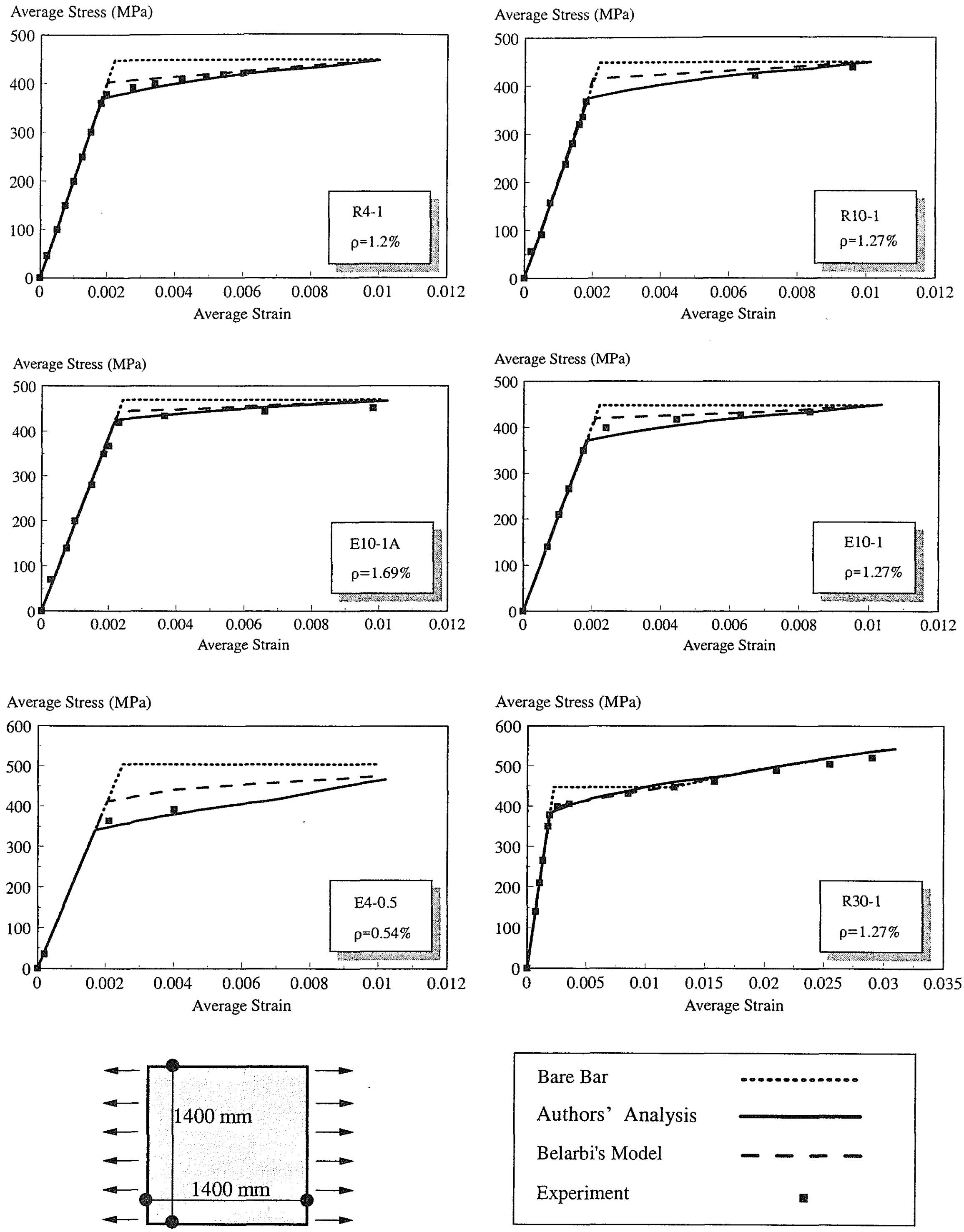

Fig. 14 Average response of re-bars: A comparison with the experimental and theoretical work of Belarbi and Hsu [6]

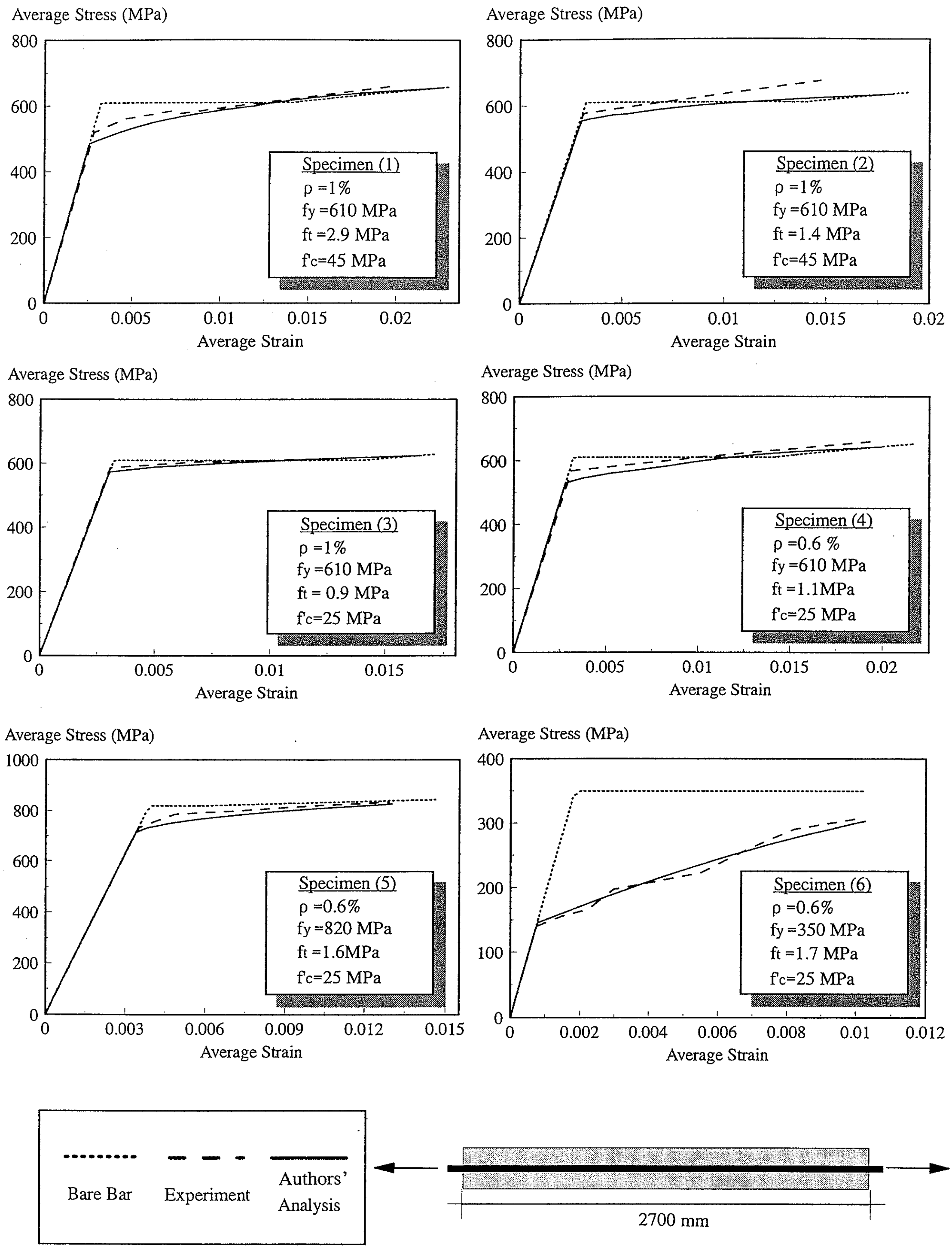

Fig. 15 Average response of reinforcement: A comparison with the experimental work of Shima et al.[4]

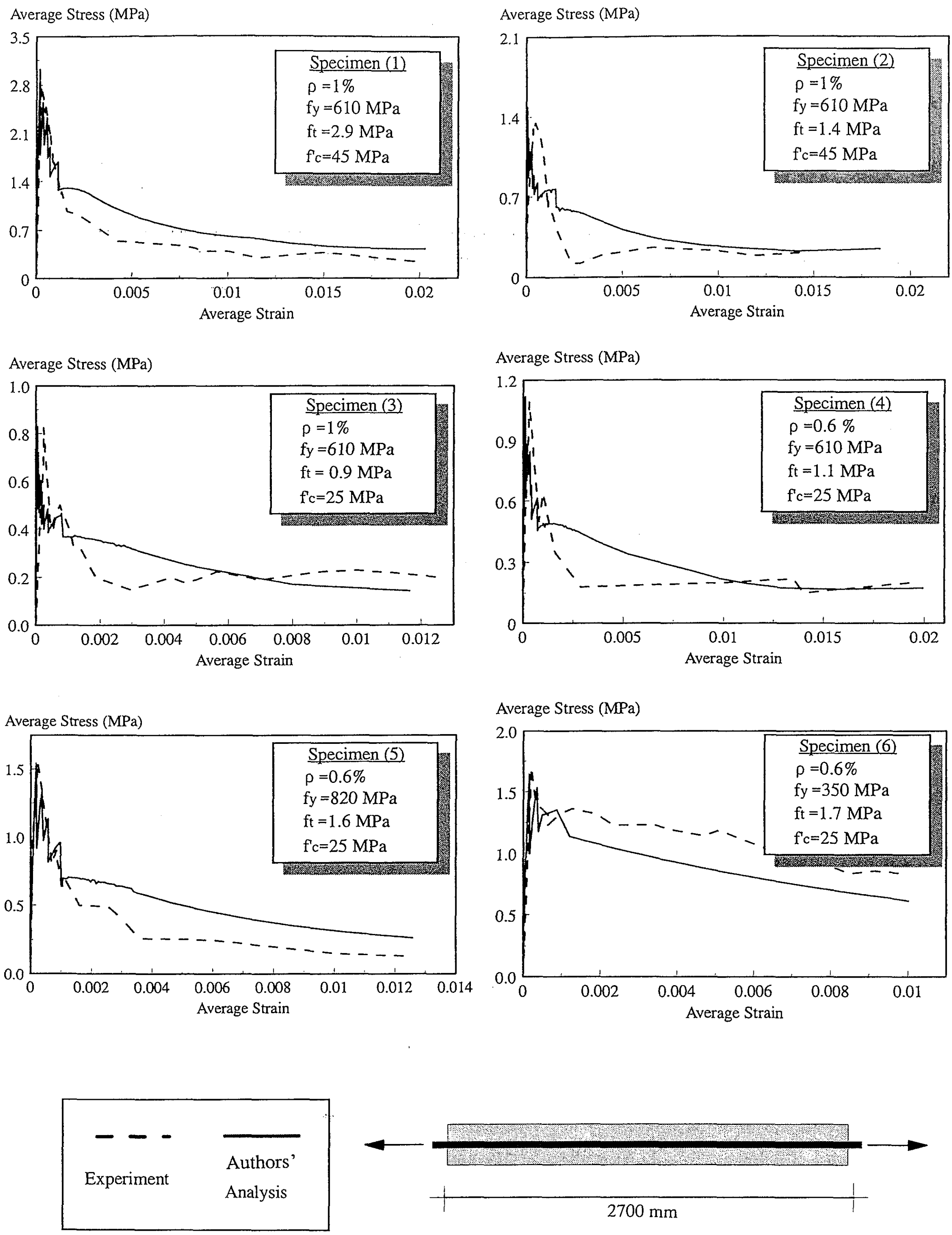

Fig. 16 Average response of concrete: A comparison with the experimental work of Shima et al.[4]

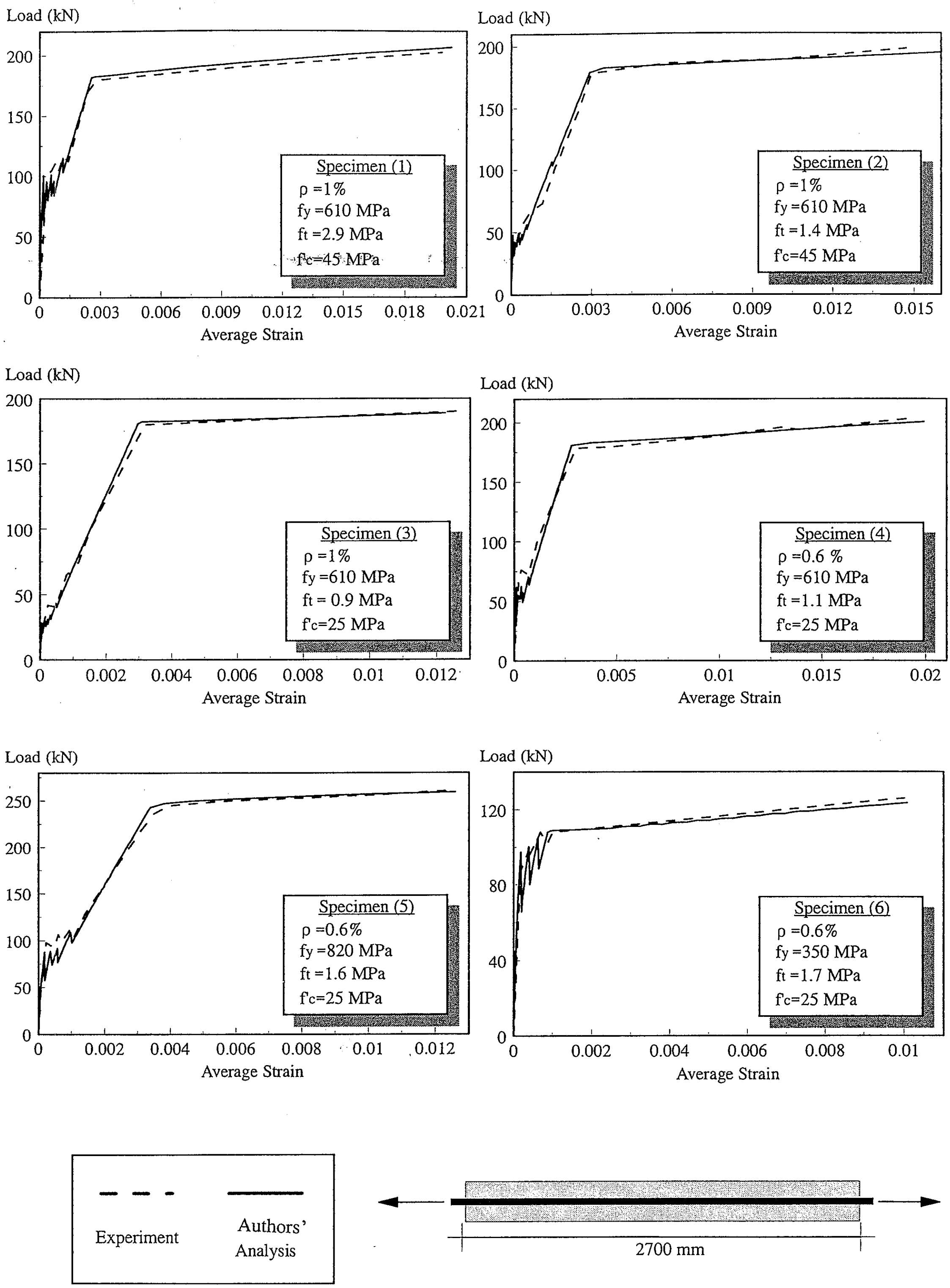

Fig. 17 Average response of RC: A comparison with the experimental work of Shima et al [4)]

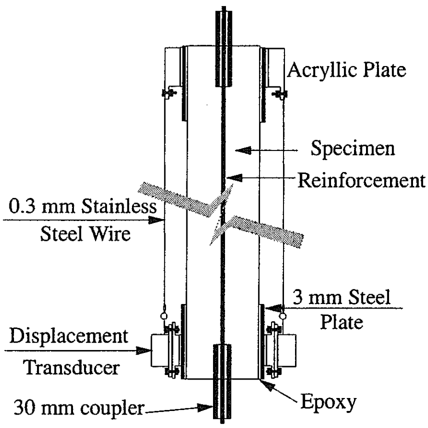

Fig. 18 Specimens' details

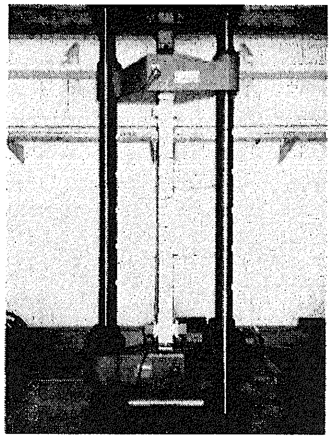

Fig. 19 Loading set-up

gripping and loading end, so as to avoid yielding of the reinforcing bars before cracking of the concrete. This was essential for specimen 3 where the yielding load is smaller than the cracking load. However, the coupler was used also in specimens 1 and 2 since the reinforcement ratio is close to the critical reinforcement ratio. The testing machine used was a universal one of 1,000 kN capacity. The loading set-up and testing machine are shown in **Fig. 19**. The total elongation of the specimen was measured using two displacement transducers on two sides of the specimen. The displacement transducers were attached to 3 mm steel plates affixed to the concrete face with an epoxy adhesive, as shown in **Fig. 18**. The purpose of the steel plates was to prevent any possible cracks beneath them, which would affect the transducers' readings. Three electrical strain gauges were attached to each side of the reinforcing bar at its center point and at 50 mm toward each end.

c) Test Results

The results of these experiments are shown in **Fig. 20** through **Fig. 27**. The analysis agrees fairly well with the experiments. It can thus be concluded that the crack spacing prediction is reasonable. For specimen (3), the analysis agrees with the experiment in predicting only one crack. This is due to the small reinforcement ratio used. However, the analysis computes only up to the ultimate point on the stress-strain relationship for the steel bar. Thus, the descending portion of the load is not considered in the analysis. This may explain the difference in ductility at failure between experiment and analysis. In the case of specimen (2), the descending branch is rather short compared to specimen (3). That is due to the fact that in specimen (2) there are several cracks, but reinforcement failure occurs only at one crack. Consequently, the total elongation is not much affected by the descending branch.

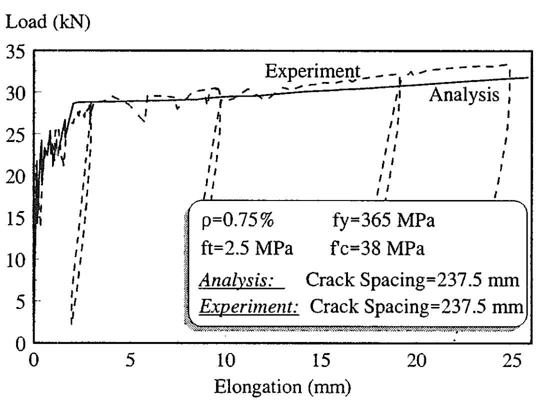

Fig. 20 Specimen(1): Experimental verification in tension

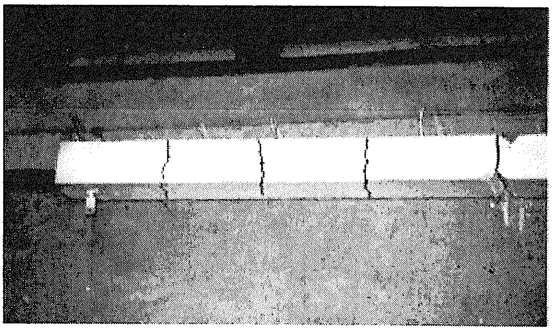

Fig. 21 Specimen(1): Observed cracking pattern

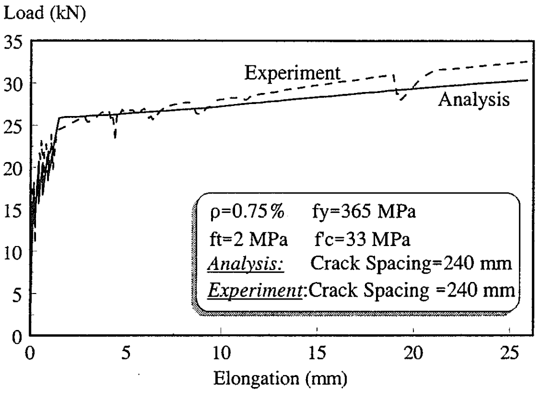

Fig. 22 Specimen(2): Experimental verification in tension

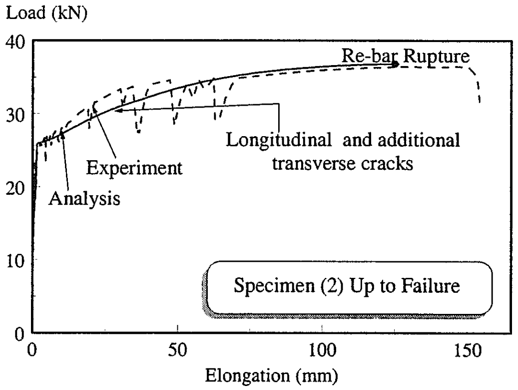

Fig. 23 Specimen(2) up to failure: Experimental verification in tension

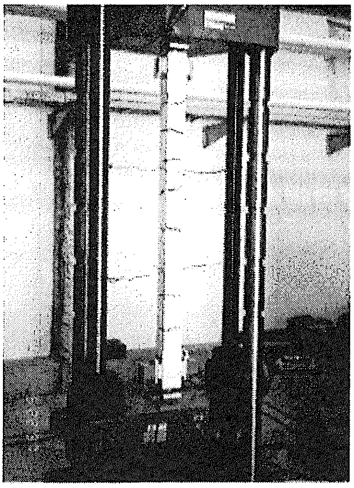

Fig. 24 Specimen(2): Observed cracking pattern

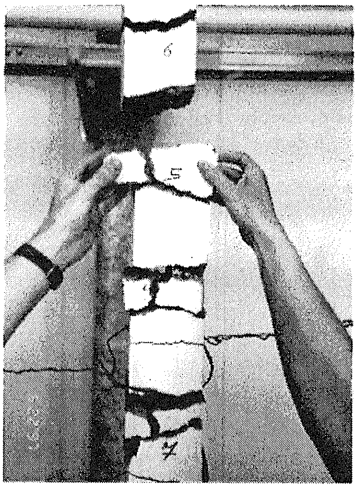

Fig. 25 Specimen(2): Observed cracking pattern at failure

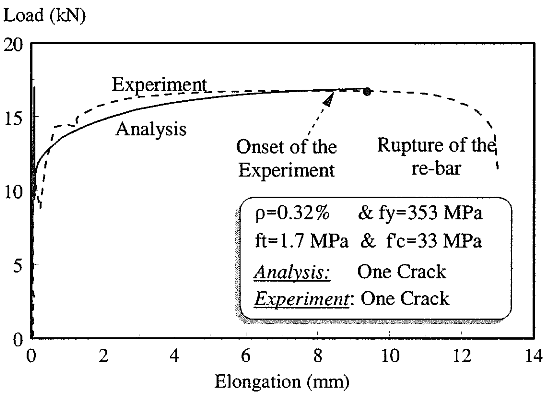

Fig. 26 Specimen(3): Experimental verification in tension

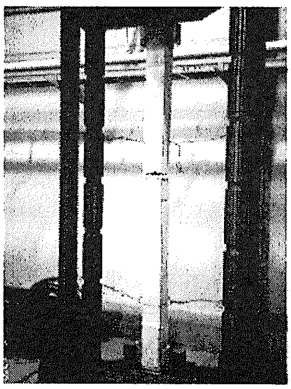

Fig. 27 Specimen(3): Observed cracking pattern at failure

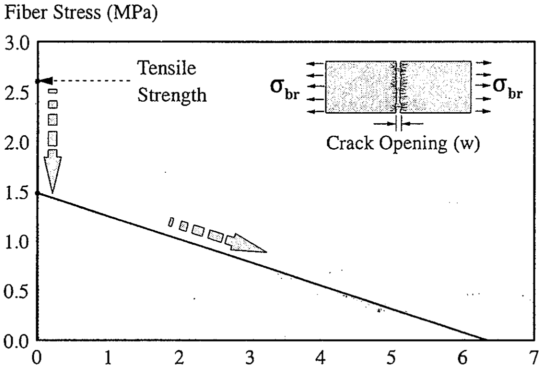

Fig. 28 Bridging stress of SFRC (Nanakorn et al. [9])

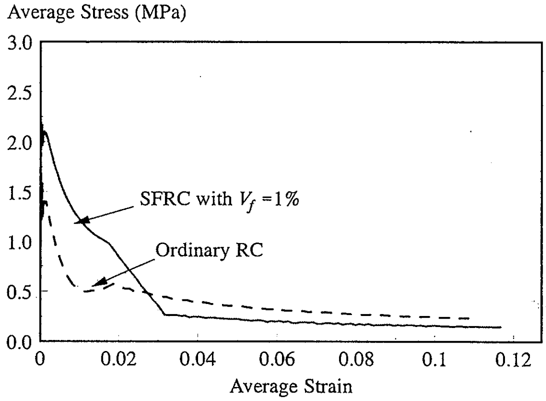

Fig. 29 Tension stiffening for SFRC

5. TENSION STIFFENING OF SFRC

When crack is generated in SFRC, the steel fibers bridge the crack and transfer tensile stress between the two portions of concrete separated by the crack. This stress transfer mechanism allows the concrete to carry more tensile force, i.e. it increases the tension stiffening of the concrete. An analysis of the tension stiffening of SFRC can be carried out in a similar manner to that described in chapter 3. If the bridging fiber stress can be obtained experimentally as a function of the crack width, the tension stiffening can be analyzed as shown in **Fig. 28** and **Fig. 29**.

As an example, **Fig. 29** shows the analysis of two tension members having the same reinforcement ratio. One of them is ordinary RC, while the other is SFRC. The bridging stress of the fibers was determined experimentally as shown in **Fig. 28**. In spite of the fact that the tensile strength of SFRC is higher than that of normal RC, the tensile strength of both RC and SFRC was intentionally assumed to be the same in order to discuss the effect of fibers on tension stiffening and ductility regardless of material strength. It is very clear that, at an average strain of 3%, the tension stiffening of SFRC falls below that of ordinary RC. This can be explained by the fact that, in the SFRC specimen, the existence of fibers causes more stress to be carried by the concrete, hence more cracks develope. At an average strain of 3%, the bridging stress becomes zero due to cut and/or pullout of the fibers. Thus, the tension stiffening at that moment depends only on the crack spacing; the smaller the crack spacing the smaller the tension stiffening. However, since in reality the tensile strength of SFRC is higher than that of ordinary RC, the crack spacing may be larger in the case of SFRC, leading to higher tension stiffening even after the cut and/or pullout of the fibers.

6. CONCLUSIONS

The conclusions of this paper can be summarized as follow:

1) Based on the microscopic bond-slip-strain model in combination with bond deterioration and tension softening at the crack surface, the stress profile and the strain profile of a reinforcing bar embedded in concrete can be computed. Hence, the macro average stress-average strain relationship of reinforcing bars as well as the tension stiffening of concrete can be computed. Thus, from the microscopic behavior of reinforced concrete, the macroscopic behavior can be deduced.
2) Using a simple stress-based method, the average crack spacing can be effectively computed.
3) In the analysis, the ultimate average strain can also be computed.
4) In reinforced concrete members with ordinary reinforcement ratios, tension softening at the crack surface can be neglected without significant influence on the average response of the concrete and reinforcement. However, in very lightly reinforced concrete or plain concrete, tension softening at fractured crack planes is predominant and has to be taken into consideration
5) The analysis can also compute the average response of SFRC taking into consideration the bridging stress transferred through the steel fibers.

References

[1] Goto, Y.: Cracks formed in concrete around deformed tension bars, *ACI Journal*, Proceedings Vol. 68, No. 4, pp. 244-251, 1971.

[2] Floegl, H. and Mang, H.: Tension stiffening concept based on bond slip, *J. of Structural Div., ASCE*, Vol. 108, No. ST12, 1982.

[3] Rizkalla, S. and Hwang, L.: Crack prediction for members in uniaxial tension, *ACI Journal*, Proceedings Vol.81, No.44, pp. 572-579, 1984.

[4] Shima H., Chou L. and Okamura, H.: Micro and macro models for bond in reinforced concrete, *Journal of The Faculty of Engineering,* The University of Tokyo (B), Vol. 39, No 2, pp. 133-194, 1987.

[5] Okamura, H. and Maekawa, K.: *Nonlinear Analysis And Constitutive Models of Reinforced Concrete*, Gihodo, Tokyo, 1991.

[6] Belarbi, A. and Hsu, T.: *Constitutive Laws Of Reinforced Concrete in Biaxial Tension-Compression*, Research Report UHCEE 91-2, University of Houston, Department of Civil and Environmental Engineering, 1991.

[7] Uchida, Y., Rokugo, K. and Koyanagi, W.: Determination of tension softening diagrams of concrete by means of bending tests, *Proceedings of JSCE,* Vol. 14, No. 426, pp. 203-212, 1991.

[8] Qureshi, J. and Maekawa, K.: Computational model for steel bar embedded in concrete under combined axial pullout and transverse shear displacement, *Proc. of JCI*, Vol.15, No. 2, pp 1249-1254, 1993.

[9] Nanakorn, P., Horii, H. and Matsuoka, S.: A fracture mechanics-based design method for SFRC tunnel linings, *J. of Materials, Conc. Struct., Pavements*, Vol.30, No.532, pp. 221-233, 1996.

[10] Salem, H. and Maekawa, K.: Tension stiffness for cracked reinforced concrete derived from micro-bond characteristics, *Proc. of JCI*, Vol.19, No.2, pp. 549-554, 1997.

[11] Salem, H. and Maekawa, K.: Computational model for tension stiffness of cracked reinforced concrete derived from micro-bond characteristics, *Proc. Of the Sixth East Asia-Pacific Conference on Structural Engineering & Construction*, Taipei, Vol.3 ,pp. 1929-1934, 1998.